Resonant-photoemission investigation of the Heusler alloys Ni_2MnSb and NiMnSb

S. W. Robey, L. T. Hudson, and R. L. Kurtz
National Institute of Standards and Technology, Gaithersburg, Maryland 20899
(Received 27 March 1992; revised manuscript received 29 June 1992)

Photoemission was used to investigate the electronic density of states (DOS) in Ni_2MnSb and NiMnSb. Comparisons with calculated band structures reveal reasonable agreement, but there are indications that the calculations overemphasize Ni $3d$ contributions at some binding energies. Resonant effects at the Mn $3p$ core threshold were employed to obtain information on the Mn $3d$ partial densities of states and these indicate that Mn $3d$ character is spread throughout the valence bands, in agreement with theory. These effects are strongest in the bottom of the valence band around a binding energy of 3.1 eV and produce structure which agrees well with the theoretical Mn $3d$ DOS, but are weak for other portions of the calculated Mn DOS. These results are discussed in the context of models for the formation of localized moments in these materials.

I. INTRODUCTION

Interest in Heusler alloys (X_nMnY where $n=1$ or 2 and X=Cu, Ni, Co, Pt, etc., Y=Sn, In, Sb, etc.) has been stimulated recently by theoretical predictions of half-metallic character[1] and the observation of very large magneto-optic effects in PtMnSb and NiMnSb.[2] A prominent characteristic of these materials, recognized from previous experimental studies,[3–7] is their local-moment character with the full magnetic moment of approximately $4\mu_B$ confined to the Ms site (with the exception of the X=Co alloys). Understanding the manner in which the local moments are formed and how they interact with the conduction electrons is a prerequisite to understanding the interesting and diverse magnetic, magneto-optic, and transport properties of these materials.

Generally the local moments have been described within a framework of virtual bound states derived from the Ms $3d$ states.[8,9] This description, usually associated with dilute alloy systems, has been justified on the basis of the large ($\sim$0.45-nm) separation between Mn atoms.[10] Attempts to model magnetic properties within this framework have been hampered by a lack of information on the electronic structure. In addition, for cases where self-consistent calculations have been performed, this localized picture of the Ms $3d$ states was challenged. Kubler *et al.* interpreted their calculations for a variety of Heusler alloys as indicating that the Mn and X element $3d$ electrons form a strongly hybridized and delocalized band.[11,12] They suggested that local moments are formed from these completely delocalized X and Mn $3d$ electrons by the exclusion of minority electrons from Mn sites rather than by localization of Mn $3d$ states.[12] This description was echoed by da Silva, Jepsen, and Andersen[13] in their studies of Ni_2MnY (Y=In, Sb, and Sn) alloys.

With these disparate views of the moment formation and underlying electronic structure in mind, we have used photoemission to probe the valence electron states in the Heusler alloys Ni_2MnSb and NiMnSb. Ni_2MnSb is a ferromagnetic alloy with an $L2_1$ crystal structure while NiMnSb has a $C1_b$ structure and is predicted to be a half-metallic ferromagnet.[1] The $L2_1$ structure can be visualized as four interpenetrating face-centered-cubic (fcc) sublattices with Ni atoms on two sublattices and Mn and Sb each occupying one of the other two. The $C1_b$ structure is formed by removing the Ni atoms from one sublattice.

Synchrotron radiation was used as an excitation source for photoemission studies. Resonant photoemission effects at the Mn $3p$ threshold were employed to obtain information on the Mn $3d$ partial density of states (DOS). In agreement with calculations, the data suggest hybridization between Mn $3d$ and Ni $3d$ states. However, there is evidence that the calculations overemphasize the Ni $3d$ contribution at the bottom of the valence bands. Corresponding differences in the resonant-photoemission behavior between Mn $3d$ states located in this region and those closer to the Fermi level are observed. An explanation of these factors is offered based on reduced hybridization between Ni $3d$ and Mn $3d$ states in the bottom of the band. No significant differences in the Mn $3p$ resonant-photoemission data from the two alloys were observed, but these measurements are probably not sensitive to changes in the interaction between Sb $5p$ and Mn $3d$ states close to the Fermi level which are predicted to signal the half-metallic character in NiMnSb.[14]

The remainder of this paper is organized as follows. Experimental details are presented in Sec. II. Nonresonant-photoemission data are presented and discussed in Sec. III, while resonant-photoemission effects are described in Sec. IV. A discussion of these results and conclusions are offered in Sec. V.

II. EXPERIMENTAL DETAILS

Samples of Ni_2MnSb and NiMnSb were obtained from the Magnetic Materials Group at the National Institute of Standards and Technology (NIST). Details of the production of the alloys are contained in Ref. 15. The sam-

ples were polycrystalline and x-ray diffraction indicated that the materials were single phase. Following ultrasonic cleaning in solvents, they were mounted in an ultrahigh-vacuum (UHV) experimental chamber equipped with a double-pass cylindrical mirror analyzer (CMA). The chamber is located on Beamline 8 at the SURF II synchrotron at NIST. A toroidal grating produced monochromatic light in the energy range from about 20 to 150 eV. The overall energy resolution of the experiment (monochromator plus electron energy analyzer) was determined using the Fermi edge from a sputtered Au foil and found to be approximately 0.4 eV at a photon energy of 40 eV. The Au foil was also used to locate the Fermi level in the alloy. Sample cleaning was accomplished by scraping with a diamond file. Photoemission spectra obtained from surfaces produced in this manner were reproducible and Auger spectra indicated only Ni, Mn, and Sb. No changes in the photoemission spectra were observed after a period of several hours in vacuum (approximately 1×10^{-10} Torr). Evidence that scraped surfaces had the appropriate bulk composition was obtained by comparing the relative core-level intensities from several alloys with varying bulk compositions (Ni_2MnSb, NiMnSb, and $Ni_{0.5}MnSb$). The relative intensities scaled correctly from one alloy to the next within the experimental uncertainty, suggesting that this method produced surfaces with the correct composition.

Photoemission spectra were acquired in an angle-integrating mode. Variation of the structure with sample rotation was checked to ensure that there was no angular dependence, implying that the angle integration was sufficient to allow the data to be compared to calculated densities of states. Also, the shape of the valence bands did not change significantly for either material over the photon energy range from 45 to 130 eV (ignoring resonant effects near the Mn 3*p* and Ni 3*p* thresholds). Thus final-state band-structure effects should not influence the use of these spectra to provide a reasonable representation of the density of initial states.

III. NONRESONANT PHOTOEMISSION

Photoemission spectra for both alloys obtained with a photon energy of 45 eV are displayed in Fig. 1. Throughout the energy range employed in this work, the structure in the photoemission spectra are representative of the Ni and Mn 3*d* contributions to the electronic structure. Intensity due to Sb 5*p*,5*s* and Ni and Mn 3*s* electron character is at least an order of magnitude lower, due to decreased cross section and lower density of states. Based on calculations of atomic cross sections,[16] the ratio σ_{Ni}/σ_{Mn} is expected to be approximately 1 for photon energies around 40–50 eV. To facilitate comparisons, the spectra in Fig. 1 have been scaled so that the valence bands (after background subtraction) are normalized to the approximate numbers of 3*d* electrons in each material ($\sim$23 in Ni_2MnSb and $\sim$14 in NiMnSb).

It is instructive to compare the photoemission data obtained for these alloys with experimental results for Ni and binary Ni alloys.[17] At least in the case of Ni_2MnSb, where the photoemission at photon energies around 45 eV is heavily dominated by the Ni 3*d* contribution, the observed shift of the peak in the valence band toward higher binding energy and the lower density of states near the Fermi level compared with elemental Ni could be interpreted according to Ref. 17 as evidence of hybridization and filling of the Ni 3*d* bands. Also the many-body satellite normally observed in Ni and Ni compounds is very weak in both of these materials, which again according to the work of Ref. 17 could be interpreted as evidence for filling of the Ni 3*d* bands through hybridization.

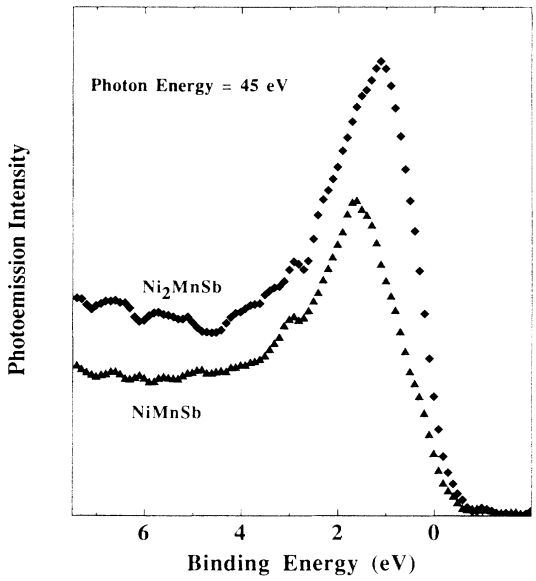

FIG. 1. Comparison between photoemission spectra for Ni_2MnSb and NiMnSb taken at a photon energy of 45 eV. The spectra have been scaled as discussed in the text.

Comparisons of the data to theoretical results are presented in Fig. 2. The peak intensity in the calculated DOS and the respective photoemission data (after background subtraction) have been set approximately equal so that the similarities and differences in the overall shapes of the theoretical and experimental results are evident. The theoretical density of states (DOS) in Fig. 2(a) for Ni_2MnSb was taken from a linear muffin-tin orbital (LMTO) by da Silva, Jepsen, and Andersen.[13] A similar comparison results with the use of the appropriately shifted DOS for Ni_2MnSn from the augmented-spherical-wave calculation of Kubler, Williams, and Sommers.[11] Only the Mn 3*d* and Ni 3*d* contributions are included in the theoretical DOS and these were convoluted with a 1-eV Gaussian to simulate intrinsic and experimental broadening processes. Because the structure is dominated by the 3*d* electron states, the use of the full DOS provides a nearly identical comparison as far as the shape of the band is concerned. For NiMnSb in Fig. 2(b), the LMTO calculations of Kulatov and Mazin[18] are presented, again with Gaussian broadening. In this case, the partial DOS were not available but, as stated above, it is expected that comparison with the primarily 3*d* contri-

bution obtained in the photoemission is still valid.

The general agreement is reasonable, particularly for NiMnSb, but the calculated bandwidth is larger for both Ni_2MnSb and NiMnSb than observed in the data. The difference is particularly strong for Ni_2MnSb. Inspection of the calculated partial DOS reveals that the structure at higher binding energy in Ni_2MnSb is primarily derived from additional Ni $3d$ contributions in the bottom of the band. Similar differences are observed in other alloys and pure transition metals, and varying explanations including the effect of matrix elements[19] and nonconstant broadening[20] (due to Auger lifetime) have been offered. However, examination of the magnitude of the modifications induced when these effects are included suggests that the differences observed here are too large to account for in this manner, at least for Ni_2MnSb.[19,20]

An alternative way of examining this set of data is to compare the differences for the two materials as observed in the photoemission with those expected based on the calculations. The theoretical treatments are the same, both being LMTO calculations employing a von Barth–Hedin approximation for exchange and correlation, so they should provide a very good comparison. Whereas the photoemission-derived DOS is similar for the two alloys, with primarily a shift of the peak to higher binding in NiMnSb, there is a significant difference in the shapes of the theoretical DOS for the two materials. Figure 3(a) presents a comparison be-

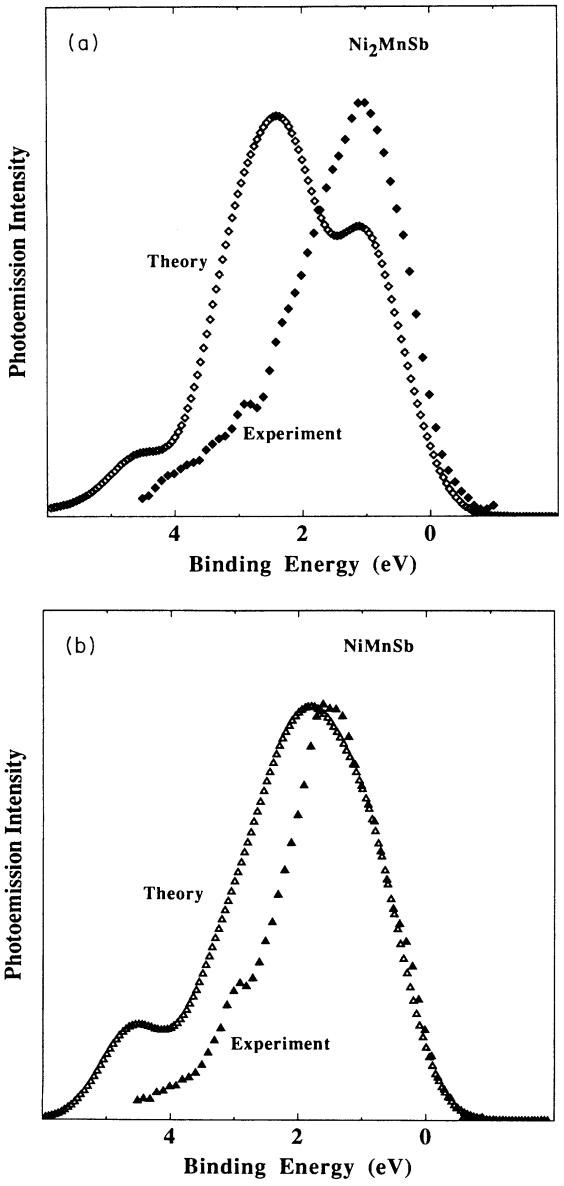

FIG. 2. Comparison between photoemission spectra and calculated DOS for (a) Ni_2MnSb (theoretical DOS from Ref. 13) and (b) NiMnSb (theoretical DOS from Ref. 18).

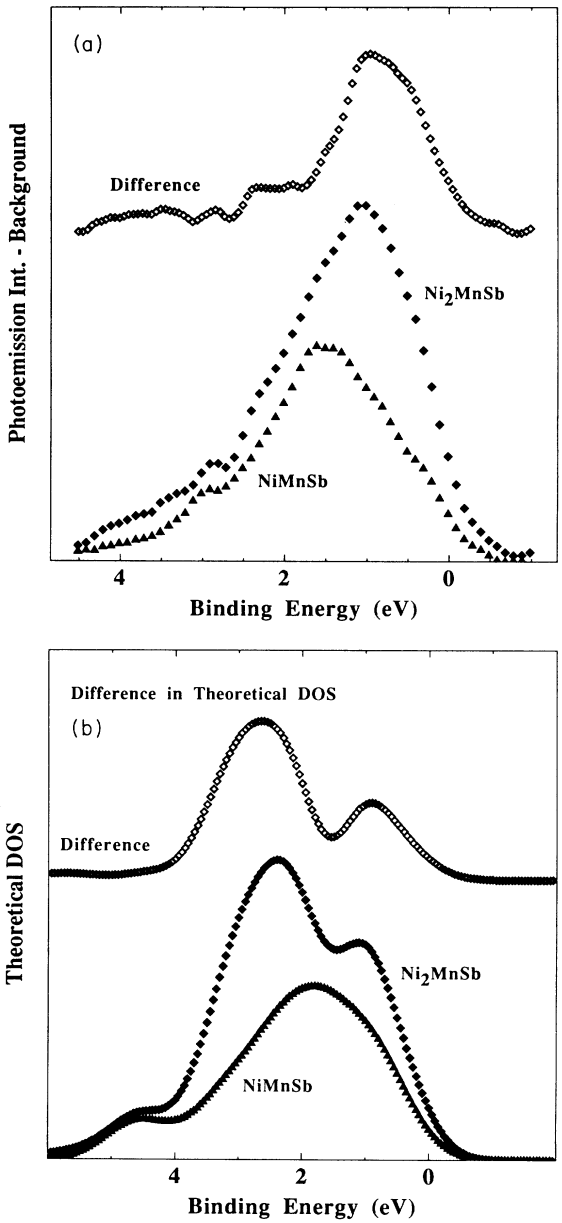

FIG. 3. (a) Comparison between photoemission spectra for Ni_2MnSb and NiMnSb. Upper curve gives the difference curve. (b) Comparison between calculated DOS for Ni_2MnSb and NiMnSb. Upper curve provides the difference in DOS between the two materials.

tween photoemission data for the two alloys along with the difference curve for the two spectra. The corresponding comparison and difference curve for the theoretical DOS is provided in Fig. 3(b). The data and calculations have been scaled to produce the correct ratio of 3*d* electrons, as described previously. The intent of this figure is to provide a qualitative idea of the changes which occur on going from Ni_2MnSb to NiMnSb. The photoemission data imply that contributions from additional Ni 3*d* states affect almost exclusively the region of the valence bands within about 2 eV of E_f. The experimentally observed shift of the intensity maximum to higher binding energy in NiMnSb is then due to the loss of this intensity at lower binding energy. Contrary to this, the theoretical comparison suggests that the influence of additional Ni states is spread throughout the band. The small intensity increase centered at a binding energy of about 1 eV agrees well with the intensity increase found in the ultraviolet photoemission spectroscopy (UPS) difference curve, but there is a much larger effect at the bottom of the band where the experimental comparison indicates virtually no change. There is some uncertainty in scaling the data which will affect the difference curve, but this will not alter the large discrepancy in the relative weighting of the observed changes in the upper and lower portions of the band structure.

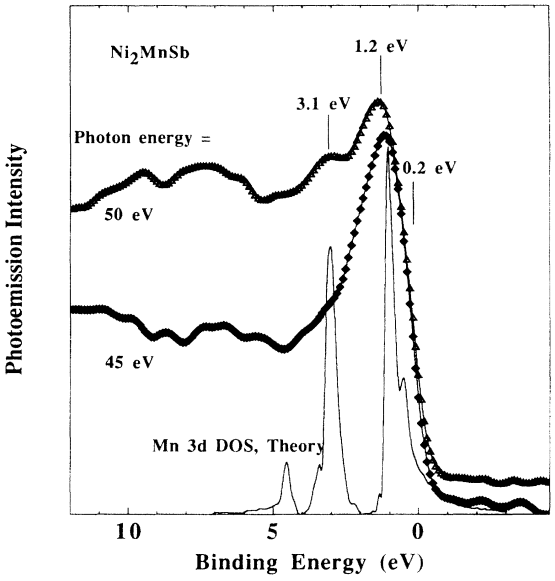

FIG. 4. Comparison between photoemission spectra for Ni_2MnSb taken at photon energies of 50 eV, the peak of the Mn 3*p* resonance, and prior to the resonance at 45 eV. The strong resonance at 3.1 eV is clearly evident. The calculated partial density of states for Mn 3*d* electrons taken from Ref. 13 is included.

IV. RESONANT PHOTOEMISSION

Resonant photoemission has been discussed extensively in the literature.[21,22] Briefly, photoemission intensity modulations are observed which arise from many electron processes accompanying excitation of, for example, a Mn 3*p* core electron to a quasidiscrete, empty 3*d* state. This followed by autoionization, which fills the 3*p* hole and ejects a continuum electron from the 3*d* portion of the valence bands. This process interferes with the first-order excitation of an electron from the filled 3*d* states directly to the continuum. The interference appears as a modulation in the photoemission intensity from regions which contain Mn 3*d* character as the photon energy is swept across the Mn 3*p* core threshold. The interference is strong for the 3*d* component at the 3*p* core edge because super-Coster-Kronig matrix elements involved in the coherent autoionization or direct recombination process are large for these transitions. In addition these matrix elements, which include the localized core hole, have short-range components. This implies that, similar to the case of core-valence-valence Auger transitions,[23] a local density of states will be sampled by the resonance. In the case of a compound material, it might be expected that resonant photoemission would produce modulations of regions more closely related to the local, or site-projected, density of states around the initial core hole than the total DOS.

Figure 4 illustrates resonant effects observed in Ni_2MnSb. A comparison is provided between photoemission spectra obtained on ($h\nu=50$ eV) and off ($h\nu=45$ eV) resonance near the Mn 3*p* core edge. Intensity modulations are particularly pronounced at the bottom of the valence bands where a weak shoulder in the off-resonant spectra develops into a rather sharp (~ 0.5 eV accounting for the experimental resolution), well-defined peak at a binding energy of 3.1 eV for 50-eV photon excitation. Modulations of the intensity in the region below ~ 4 eV are associated with the emergence of $M_{23}VV$ Auger peaks and contributions from two-hole final states.[21]

The structure which appears at 3 eV in the 50-eV spectrum clearly indicates that the whole valence band does not modulate uniformly across the Mn 3*p* threshold. For comparison, the Mn local 3*d* partial density of states from the linear muffin-tin-orbital (LMTO) calculations of da Silva, Vepsen, and Andersen, for Ni_2MnSb is included in Fig. 4. The calculation exhibits two sharp, well-separated peaks in the DOS. The splitting between the two main features in the theory presumably arises due to crystal-field effects, so that the peak at approximately 3 eV is derived predominantly from e_g-like states. The peak closer to the Fermi level is produced by Mn 3*d* states with predominantly t_{2g} character. The position of the 3.1-eV resonant peak in the 50 eV photoemission spectrum agrees very well with the position of the high binding-energy peak in the theoretical density of states, but there does not seem to be a correspondingly strong enhancement of the Mn 3*d* structure close to the Fermi level.

To further illustrate this, Fig. 5 provides an attempt to simulate the photoemission spectrum on resonance ($h\nu=50$ eV) by combining the off-resonant spectrum ($h\nu=45$ eV) with an enhanced Mn 3*d* site-projected DOS from the calculation. However, if the theoretical Mn 3*d* DOS is scaled and added to the 45-eV spectrum to

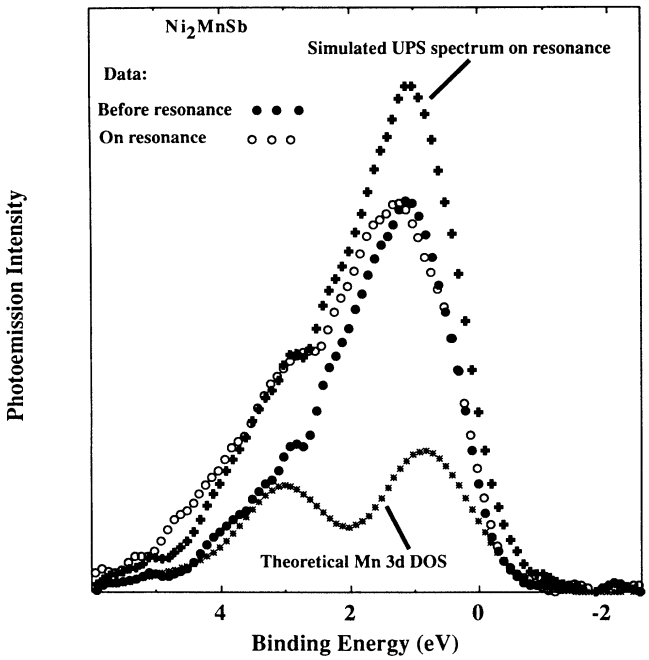

FIG. 5. This figure illustrates a simple attempt to simulate the resonant photoemission. The solid circles represent the photoemission spectrum obtained at $h\nu=45$ eV (after background subtraction). The open circles are the spectrum for $h\nu=50$ eV. The solid crosses provide the simulated spectrum obtained by adding the theoretical Mn DOS (stars) to reproduce the 50-eV spectrum at a binding energy of 3 eV.

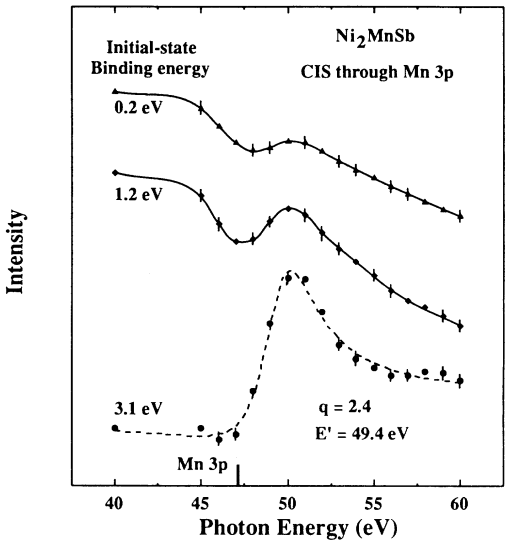

FIG. 6. Constant initial-state (CIS) scans from Ni_2MnSb for the three initial-state energies indicated by tic marks in Fig. 1. The data have been smoothed by adjacent channel averaging. The solid curves through the 0.2- and 1.2-eV data are guides for the eye. The dashed line through the 3.1-eV data is a fit to a Fano line shape as described in the text.

correctly reproduce the intensity at the bottom of the band at 50 eV, then the intensity in the region closer to the Fermi level is significantly overestimated. This cannot be attributed to a reduction in the cross section of a nonresonant Ni $3d$ contribution.[16] Thus, the spectral shape of the 50-eV data is not reproduced with this simple model. Clearly, a stronger resonant effect is produced for the region corresponding to the higher binding-energy structure in the theoretical Mn DOS than for the structure closer to E_F. Based on the idea that resonant photoemission is a local probe, a simple explanation would be a larger concentration of more localized Mn $3d$ states at binding energies near 3 eV. The lack of detailed theoretical connections between structure in the one-electron DOS and the resonance, including other factors which can influence the strength of the resonance, renders this speculative. It is clear, however, that the two components of the theoretical Mn DOS are not sampled equally in the resonant process.

To investigate the resonant structure in the region of the spectrum closer to the Fermi level more thoroughly, and provide more detail on the structure near 3 eV, constant initial-state (CIS) scans were performed for several initial state energies. Data for the three initial-state binding energies indicated in Fig. 4 are displayed in Fig. 6. The data in this figure were acquired by taking individual photoemission spectra at a series of photon energies spanning the Mn $3p$ edge. Normalization of the data for the photon flux was performed and a background representing secondary electron contributions was subtracted. The intensity within a window 0.5 eV wide centered at the binding energy of interest was integrated to increase statistics. These data were smoothed by adjacent channel averaging before presentation. The solid lines through the 0.2 and 1.2-eV data are meant to guide the eye. Fits were also performed with an additional broad Gaussion located at binding energies around 6–8 eV in an attempt to reduce the influence overlapping intensity variations evident in the region below binding energies of 4 eV which arise due to Auger transitions and contributions from two-hole final states appearing close to the resonance. Only the resonance at 3.1 eV was affected, reducing the resonant enhancement by approximately 30% in the most drastic case.

Figure 6 indicates that all three binding energies exhibit resonant effects for photon energies near the Mn $3p$ core threshold. Thus, Mn $3d$ character is spread throughout the valence bands, but the observed resonant shapes are qualitatively different. For binding energies around 3 eV a strong resonant profile is observed while the 0.2- and 1.2-eV data exhibit a weak, nearly antiresonant character. Fits to a Fano profile,[21,24]

$$I(h\nu)=I_{\rm res}[(q+\varepsilon)^2/(1+\varepsilon^2)]+I_{\rm nonres}(h\nu)\ , \qquad (1)$$

were performed for each of the CIS curves to provide an indication of the degree of difference. Here $h\nu$ is the photon energy, q, is the asymmetry parameter, and ε is the reduced energy $\varepsilon=(h\nu E')/\Gamma_{1/2}$. $\Gamma_{1/2}$ is the half-width of the resonance and E' is the energy of the resonance. Equation (1) assumes that the observed intensity consists of a resonant contribution, derived from Mn $3d$

states, and possibly a nonresonant background contribution. No strong energy-dependent behavior is expected other than that due to resonance of Mn $3d$ contributions. The nonresonant contribution to the intensity, $I_{\text{nonres}}(E)$, which accounts for primarily Ni contributions to the photoemission current as well as systematic variations in flux normalization or background removal, was modeled using various polynomial functions up to third order in $h\nu$. For the initial states at 0.2 and 1.2—near the Fermi level and at the peak of the valence bands—the value of E' was found to be ~ 49.5–49.9 eV. Values of the asymmetry parameter were $q \sim 0.5$ for the 0.2-eV data and $q \sim 1.5$ for the 1.2-eV data. The asymmetry parameter depended somewhat on the details of the fit and smoothing of the data leading to variations in q of about 30%. Fits to the resonance at 3.1 eV also produced $E' \sim 49.5$ eV but $q \sim 1.7$–2.4, depending on whether or not attempts were made to remove possible overlapping contributions to the resonance. The result of one such fit is displayed as the dashed line in Fig. 6. These fits were produced primarily to illustrate more concretely the different resonant profiles observed for different initial states. As in the comparison of the apparent size of the resonant effect, the CIS data and parameters obtained from it indicate a qualitative change between the regions of binding energy appropriate for the two structures in the calculated DOS.

Strong similarities exist between these data and results obtained in investigations of the dilute magnetic semiconductor $Cd_{1-x}Mn_xTe$ by Ley *et al.*[25] Constant initial-state data across the Mn $3p$ edge show the same trend as a function of binding energy as observed for Ni_2MnSb. A strong resonant feature was also observed at a binding energy of about 3.4 eV. This was attributed to Mn $3d$ states only weakly hybridized with Cd or Te.[25] The above parameters can also be compared with those obtained for resonances in various partial cross sections of the ^6S-^6P transition in atomic Mn [Ref. 26(a)] and absorption in metallic films of Mn.[26(b)] The values of q and E' obtained for the enhancement at 3-eV binding energy are close to the parameters deduced from Fano fits to corresponding partial cross sections in the atomic data, where q ranges from 2.2 to 2.5 and $E' = 50.0$–50.1 eV, whereas the other two initial states exhibit much weaker effects and asymmetry parameters significantly different from the atomic case. The 3-eV structure as a function of photon energy is also more similar to measured absorption profiles. Note that this includes comparisons with observations of photoemission partial cross sections in atomic Mn. Care must be exercised in comparisons solely between resonant profiles observed in photoemission and absorption.[24]

Resonant-photoemission results for NiMnSb are similar to those discussed above for Ni_2MnSb. A comparison of spectra on and off resonance is given in the top part of Fig. 7. In particular, a well-defined peak again emerges at a binding energy of about 3 eV. The corresponding CIS data for NiMnSb are displayed in the bottom portion of Fig. 7. Although the lack of data below 45 eV precludes generating unique fits, the same general trend of increasing resonant effects with increasing binding energy seen in Ni_2MnSb is found for NiMnSb. Again the 3.1-eV

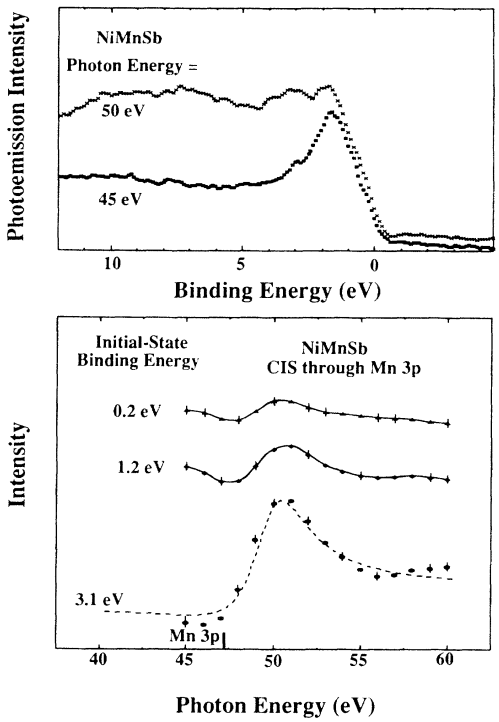

FIG. 7. The top portion of the figure displays a comparison between spectra taken before and on resonance for NiMnSb using the same photon energies as in Fig. 4 for Ni_2MnSb. The bottom of the figure gives the corresponding CIS data for NiMnSb. The solid lines through the 0.2- and 1.2-eV data are guides for the eye. The dashed line through the 3.1-eV data reproduces the fit shown in Fig. 6 for Ni_2MnSb.

CIS displays a strong resonant enhancement at the Mn $3p$ edge. The dashed line in this figure is the same fit given in Fig. 6 for the Ni_2MnSb data and it can be seen that the quality of the fit is very nearly the same. This suggests that the Mn $3d$ states in this portion of the valence bands are similar in both alloys. This agrees with the conclusion of de Groot *et al.*[1] that the band structures of the $L2_1$ and $C1_b$ alloys are very similar in many aspects.

Interference effects at the Ni $3p$ core threshold were also examined for both materials. As observed in Ni and many Ni compounds, the resonance in the "main" or screened portion of the bands displayed a weak antiresonant character whereas binding energies below ~ 5 eV show strong resonant enhancements due to the formation of correlated two-hole states.[21] For the region around 3 eV below E_F, very little effect was observed in either material. Any weak antiresonant effect in this region would overlap with strong resonant effects at slightly higher binding energies, so that it is difficult to draw firm conclusions based on these data. This would, however, support the idea that there is a small contribution from Ni $3d$ states in the lower portion of the valence bands.

V. CONCLUSIONS

Photoemission was used to investigate the electronic structure in Ni_2MnSb and NiMnSb and resonant effects

at the Mn 3*p* edge were employed to provide information on Mn 3*d* contributions. The overall picture of the electronic structure of Ni_2MnSb and NiMnSb derived from this study is in general agreement with some aspects of theoretical presentations for the same materials. There is reasonable agreement between the photoemission results and the calculated DOS, particularly in the case of the half-metallic material NiMnSb. Resonant-photoemission intensity modulations at the Mn 3*p* threshold were observed for all initial states. This agrees with the theoretical contention that Mn 3*d* character is spread over a large energy width. A strongly resonating peak at a binding energy of 3.1 eV agrees well with the calculated Mn 3*d* partial density of states in Ni_2MnSb. A nearly identical resonant feature is observed in NiMnSb.

However, several puzzling aspects were noted. Comparisons between photoemission and the calculated DOS reveal a somewhat larger bandwidth. For Ni_2MnSb there is a noticeably larger contribution to the bottom of the valence band in the calculation. This appears to be due to additional contribution from Ni 3*d* states at these energies. The photoemission difference curve between Ni_2MnSb to NiMnSb indicates that Ni 3*d* states contribute primarily in the region from E_F to about 2 eV, rather than throughout the whole band as in the calculation. These factors suggest a lower contribution from Ni 3*d* states at the bottom of the band than indicated in the calculation, at least in the case of Ni_2MnSb.

Weaker resonant effects and different resonant structure are observed for binding energies close to E_F than for structure around 3 eV. A possible explanation was offered in terms of more localized, less hybridized Mn 3*d* states at this energy. This would be consistent with the idea that there is a small contribution from Ni 3*d* states in this region and the similarity in the resonance observed at 3 eV to that in elemental Mn. In the limit of no hybridization, it is expected that the Mn states would resonate with a profile similar to that observed for atomic and metallic Mn, as observed at 3 eV. Previous work has indicated that the shape and intensity of the resonance can be affected by initial-state hybridization[27–30] and this could explain the changes observed for lower initial-state energies, but a detailed, systematic investigation has not been performed. The possibility that other aspects of the resonant process (other than initial-state hybridization) lead to the observed behavior cannot be ruled out. The same resonance energy was obtained for all initial states, which suggests that the intermediate state involved is the same in each case. The significant point is, however, that there is a noticeable difference in the behavior of the different components obtained in the calculated DOS in terms of participation in the resonance.

It is clear, based on these results, that a classic picture for the formation of the local moments, consisting of a single, well-defined virtual bound state, is not correct. The Mn 3*d* states are indeed spread over a large energy range and the states near E_F are degenerate with a high density of Ni 3*d* states. However, the justification behind a picture with a completely delocalized 3*d* band was based largely on the fact that the total bandwidth over which Mn 3*d* states were spread is large and similar to the Ni 3*d*-band width, even though the calculation shows two sharp, well-separated features.[13] The different resonant behavior for regions of binding energy corresponding to these two structures suggests the possibility that they could be considered in some sense as separate bands. In this case the relevant parameter becomes the bandwidth of the individual peaks. Thus, even considering the uncertainty in arriving at a detailed interpretation of the resonant effects, these observations suggest that the picture of a common, completely delocalized band for the Ni and Mn 3*d* electrons may also be too simplistic. In this regard, it is also interesting to note that the Mn 3*d* DOS calculated for the Heusler alloy Cu_2MnAl in Ref. 11 is very similar to the Mn 3*d* DOS calculated by Podloucky, Zeller, and Dederichs for an Mn impurity in Cu.[31] Whereas Ref. 11 described Cu_2MnAl in strongly hybridized, delocalized limit, the Mn impurity DOS in Ref. 31 is described as a virtual bound state modified somewhat by interaction with the Cu host.

The differences between the $L2_1$ alloy and the $C1_b$ alloy observed in this study cannot be interpreted easily to shed light on the possibility of half-metallic character in NiMnSb. Based on the discussion of de Groot *et al.* for NiMnSb, the Mn 3*d* levels of predominantly e_g symmetry should show little effect of the change in symmetry between the two crystal structures, and this is consistent with the assignment of the peak at 3 eV as predominantly 3*d* e_g derived. The position and resonant behavior of this feature is the same in both materials to within the experimental uncertainty. No spectral changes that could clearly be linked to differences in the Mn 3*d*–Sb 5*p* hybridization near the Fermi level, predicted to be a signature of the formation of the half-metallic band structure, were evident. However, as stated above, due to the dominance of the Ni 3*d* contribution close to E_F and the lack of sensitivity to the Sb contribution, it is doubtful if these measurements would be sensitive to changes at this level.

ACKNOWLEDGMENTS

We wish to thank the members of the Magnetic Materials Group at NIST for providing the samples and the staff at the SURF II synchrotron for assistance with these measurements.

[1]R. A. de Groot, F. M. Mueller, P. G. van Engen, and K. H. J. Buschow, Phys. Rev. Lett. **50**, 2024 (1983).

[2]P. G. van Engen, K. H. J. Buschow, R. Jongbreur, and M. Erman, Appl. Phys. Lett. **42**, 202 (1983); R. A. de Groot, F. M. Mueller, P. G. van Engen, and K. H. J. Buschow, J. Appl. Phys. **55**, 2151 (1984); R. Ohyama, T. Koyanagi, and K. Matsubara, *ibid.* **61**, 2347 (1987).

[3]F. A. Hames and J. Crangle, J. Appl. Phys. **42**, 1336 (1971).

[4]K. R. A. Ziebeck and P. J. Webster, J. Phys. Chem. Solids **35**, 1 (1974).

[5]C. C. M. Campbell, J. Phys. F **5**, 1931 (1975).

[6]A. Hamzic, R. Asomoza, and I. A. Campbell, J. Phys. F **11**,

1441 (1981).
[7]P. J. Webster, Contemp. Phys. **10**, 559 (1969).
[8]J. Friedel, Can. J. Phys. **34**, 1190 (1956).
[9]P. W. Anderson, Phys. Rev. **124**, 41 (1961).
[10]G. Gruner, Adv. Phys. **23**, 941 (1974), and references therein; T. Kaysuya, Solid State Commun. **15**, 1119 (1974); G. Malmstrom, D. J. W. Geldart, and C. Blomberg, J. Phys. F **6**, 233 (1976); **6**, 1953 (1976); D. C. Price, *ibid.* **8**, 933 (1978).
[11]J. Kubler, A. R. Williams, and C. B. Sommers, Phys. Rev. B **28**, 1745 (1983).
[12]A. R. Williams, V. L. Moruzzi, C. D. Gelatt, and J. Kubler, J. Magn. Magn. Mater. **31-34**, 88 (1983).
[13]E. Z. da Silva, O. Jepsen, and O. K. Andersen, Solid State Commun. **67**, 13 (1988).
[14]J. Kubler, Physica **127B**, 257 (1984).
[15]L. J. Swartzdruber and B. J. Evans, in *Magnetism and Magnetic Materials 1971,* Proceedings of the 17th Annual Conference on Magnetism and Magnetic Materials, edited by D. C. Graham and J. J. Rhyne, AIP Conf. Proc. No. 5 (AIP, New York, 1972), p. 539.
[16]J. J. Yeh and I. Lindau, At. Data Nucl. Data Tables **32**, 1 (1985).
[17]J. C. Fuggle, F. U. Hillebrecht, R. Zeller, Z. Zolnierek, P. A. Bennett, and Ch. Freiburg, Phys. Rev. B **27**, 2145 (1982).
[18]E. Kulatov and I. I. Mazin, J. Phys. Condens. Matter **2**, 343 (1990).
[19]N. V. Smith, G. K. Wertheim, S. Hufner, and M. M. Traum, Phys. Rev. B **10**, 3197 (1974).
[20]P. J. Durham, W. M. Temmerman, and A. M. Begley, in *Auger Spectroscopy and Electronic Structure,* edited by G. Cubiotti, G. Mondio, and K. Wandelt (Springer-Verlag, Berlin, 1989), p. 57.
[21]U. Fano, Phys. Rev. **124**, 1866 (1961); L. C. Davis, J. Appl. Phys. **59**, R25 (1986), and references therein.
[22]J.-C. Parlebas, A. Kotani, and J. Kanamori, J. Phys. Soc. Jpn. **51**, 124 (1982); J.-C. Parlebas, A. Kotani, and J. Kanamori, Solid State Commun. **41**, 439 (1982).
[23]R. Weissmann and K. Muller, Surf. Sci. Rep. **1**, 251 (1981).
[24]Y. Yafet, Phys. Rev. B **21**, 5023 (1979).
[25]M. Taniguchi, L. Ley, R. L. Johnson, J. Ghijsen, and M. Cardona, Phys. Rev. B **33**, 1206 (1986); L. Ley, M. Taniguchi, J. Ghijsen, R. L. Johnson, and A. Fujimori, *ibid.* **35**, 2839 (1987).
[26](a) E. Schmidt, H. Schroder, B. Sonntag, H. Voss, and H. E. Wetzel, J. Phys. B **18**, 79 (1985); (b) B. Sonntag, R. Haensel, and C. Kunz, Solid State Commun. **7**, 597 (1969).
[27]J. Igarashi and T. Nakano, J. Phys. Soc. Jpn. **55**, 1384 (1986).
[28]L. C. Davis, Phys. Rev. B **25**, 2912 (1981).
[29]A. Kakizaki, K. Sugeno, T. Ishii, H. Sugawara, I. Nagakara, and S. Shin, Phys. Rev. B **28**, 1026 (1983).
[30]A. Fujimori and F. Minami, Phys. Rev. B **30**, 957 (1984); A. Fujimori, M. Saeki, N. Kimizuka, M. Taniguchi, and S. Suga, *ibid.* **34**, 7318 (1986).
[31]R. Podloucky, R. Zeller, and P. H. Dederichs, Phys. Rev. B **22**, 5777 (1980).